13th World Conference on Earthquake Engineering
Vancouver, B.C., Canada
August 1-6, 2004
Paper No. 367

3-DIMENSIONAL RESPONSE CHARACTERISTICS OF CONTINUOUS VIADUCT NEAR A FAULT

Koutaku OHO [1], Takanori HARADA[2] and Tetsuya NONAKA[3]

SUMMARY

This study has investigated the characteristics of the temporal and spatial variability of near field ground motions, and the characteristics of the 3 dimensional nonlinear response of inelastic continuous long viaduct. The near fault ground motions with large permanent movements due to the fault rupture are simulated by the kinematic model of fault rupture in horizontally homogeneous layered media. The effects of the sedimentary layer and the depth of the upper edge of the fault upon the ground motions, and upon the nature of inelastic response of the viaduct are examined. It is found that the seismic wave motions near a fault are quite complex, and the spatial and temporal variation looks like the vortexes appearing behind an obstacle in the air or water flow, and also found that the thickness of the sedimentary layer strongly affects on the response behaviors of the viaduct near the fault.

INTRODUCTION

During the past 70 years of strong motion observation in the seismic regions, we have little data for strong ground motions in near earthquake faults. Consequently, we know little about the characteristics of near fault ground motions, more precisely the nature of both temporal and spatial variation of near field ground motions. On the other hand, it is known that the temporal variation of ground motions affects strongly the response of inelastic structures, and also the spatial variability of ground motions may play a major role in causing damage to such extended structures as pipelines and long bridges.

This paper describes the theoretical study on the characteristics of the temporal and spatial variability of near field ground motions, and also on the characteristics of the 3 dimensional nonlinear response of inelastic continuous long viaduct to the near field ground motions. In this paper, assuming a strike slip fault, we examine the two cases; the one is a continuous viaduct crossing the fault and the other case is the continuous viaduct running parallel to the fault. The near field ground motions are simulated using a discrete three fold Fourier transform of the analytical forms of seismic wave field in frequency wave

---

[1] Graduate Student, Dept. of Civil and Environmental Engineering, Miyazaki University, JAPAN, hongze@civil.miyazaki-u.ac.jp
[2] Professor, Dept. of Civil and Environmental Engineering, Miyazaki University, JAPAN, harada@civil.miyazaki-u.ac.jp
[3] Chief, Dept. of Planning and Research, Yamatosekei Company Ltd., JAPAN, nonaka@yamato-engco.jp

number domain. They are derived by a stiffness matrices based formulation of physical processes of propagation of the seismic waves generated by the kinematic model of the fault rupture in horizontally layered media Harada, et al. [2] [3].

In the simulation of seismic ground motions, the 6 components of free field ground motions, consisting of the three translational motions (u, v, w) and the three rotational motions ($\omega_x, \omega_y, \omega_z$) around the 3 coordinate axes in the Cartesian coordinate system (x, y, z where the x and y plane corresponds to the free field ground surface, and z axis expresses the depth from the free field ground surface), are simulated. The two rotational motions (ω_x, ω_y) are the pitch, and the roll corresponding to the tilts of free field ground surface, and (ω_z) is the yaw corresponding to the rotation of the free field ground surface. Especially, the influences of the thickness of the sedimentary layer and the depth of upper edge of the fault upon the ground motions, and also, upon the response behaviors of the viaduct near the fault are investigated.

MODELS OF FAULT AND SEDIMENTARY LAYER

In this study, we use the 3 models of the fault and horizontally homogenous sedimentary layer as shown in Fig.1. The model A (ground surface fault) in Fig.1 has no sedimentary layer where the upper edge of the strike slip fault reaches to the ground surface. The models B and C have the sedimentary layers with thickness of 0.5km and 1.5km, respectively, overlaying the bedrock in which the strike slip fault rupture with rupture speed of 2.2km/sec, length of 8.5km, and width of 8.5km occurs and its upper edge reaches to the bottom of the sedimentary layer.

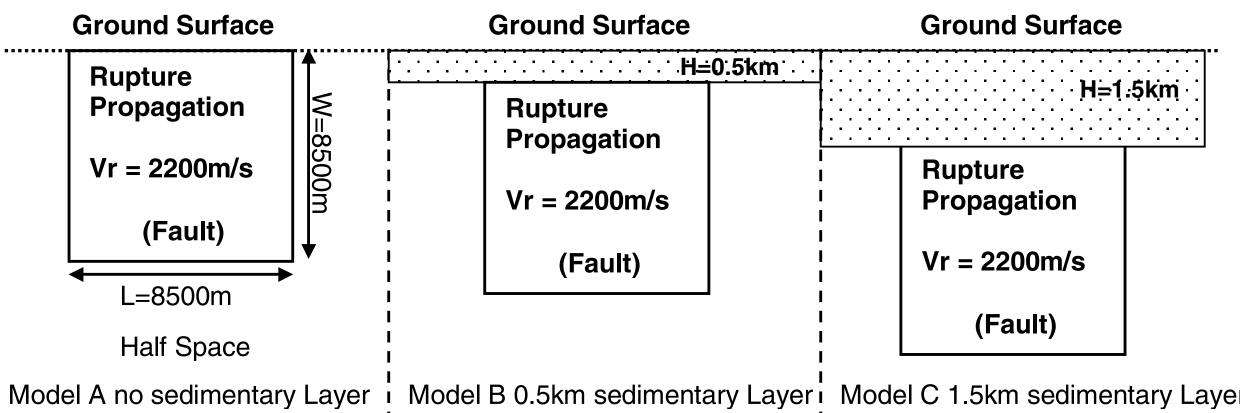

Fig. 1 Three models of fault and sedimentary layer system used in this study

Table 1 Material properties of the sedimentary layer and bedrock

Material Properties	Sedimentary layer			Half space bedrock
	ModelA	ModelB	ModelC	
Thickness of layer H (m)	0	500	1500	----
P-wave speed (m/sec)	2800	2800	2800	6000
S-wave speed (m/sec)	1600	1600	1600	3500
Density (t/m^3)	2.3	2.3	2.3	2.8
Q Value	150	150	150	400

Table 2 Parameters of the extended fault rupture

Seismic moment	$M_0 = 2.3 \times 10^{17} N \times m$
Rise time	$\tau = 0.3s$
Length of fault	$L = 8500m$
Width of fault	$W = 8500m$
Rupture speed	$v_r = 2200m/s$
Strike angle	$\phi = 0^o$
Dip angle	$\delta = 90^o$
Slip angle	$\lambda = 0^o$

The material properties of the sedimentary layer and the bedrock are shown in Table 1 and also, the parameters of the fault are shown in Table 2, which is cited from the paper Harada et al. [2][3].

COMPLEX NATURE OF SPATIAL AND TEMPORAL VARIATION OF GROUND MOTIONS NEAR A STRIKE SLIP FAULT

The ground motions with permanent ground movements due to the fault rupture are simulated using a discrete three fold Fourier transform of the analytical forms of seismic wave field in the frequency wave number domains which are derived by a stiffness matrices based formulation of the physical processes of propagation of the seismic waves generated by the kinematic model of fault rupture in horizontally homogenous sedimentary layer as shown in Fig.1, Harada et al. [2][3]. By considering the uncertainty of the details of fault sedimentary models as well as the predominant frequency (about 0.5 Hz) of the continuous viaduct, the ground motions up to 2.5Hz are simulated in this study.

To see the spatial and temporal variation of horizontal ground motion accelerations on the free field ground surface near the fault for the 3 models A, B and C of Fig.1, Fig.3 shows the snapshots of horizontal ground motion accelerations of the free field ground surface over 30km by 30km area, at 4 time instants; 1.05sec, 3.14sec, 6.28sec and 7.33sec.

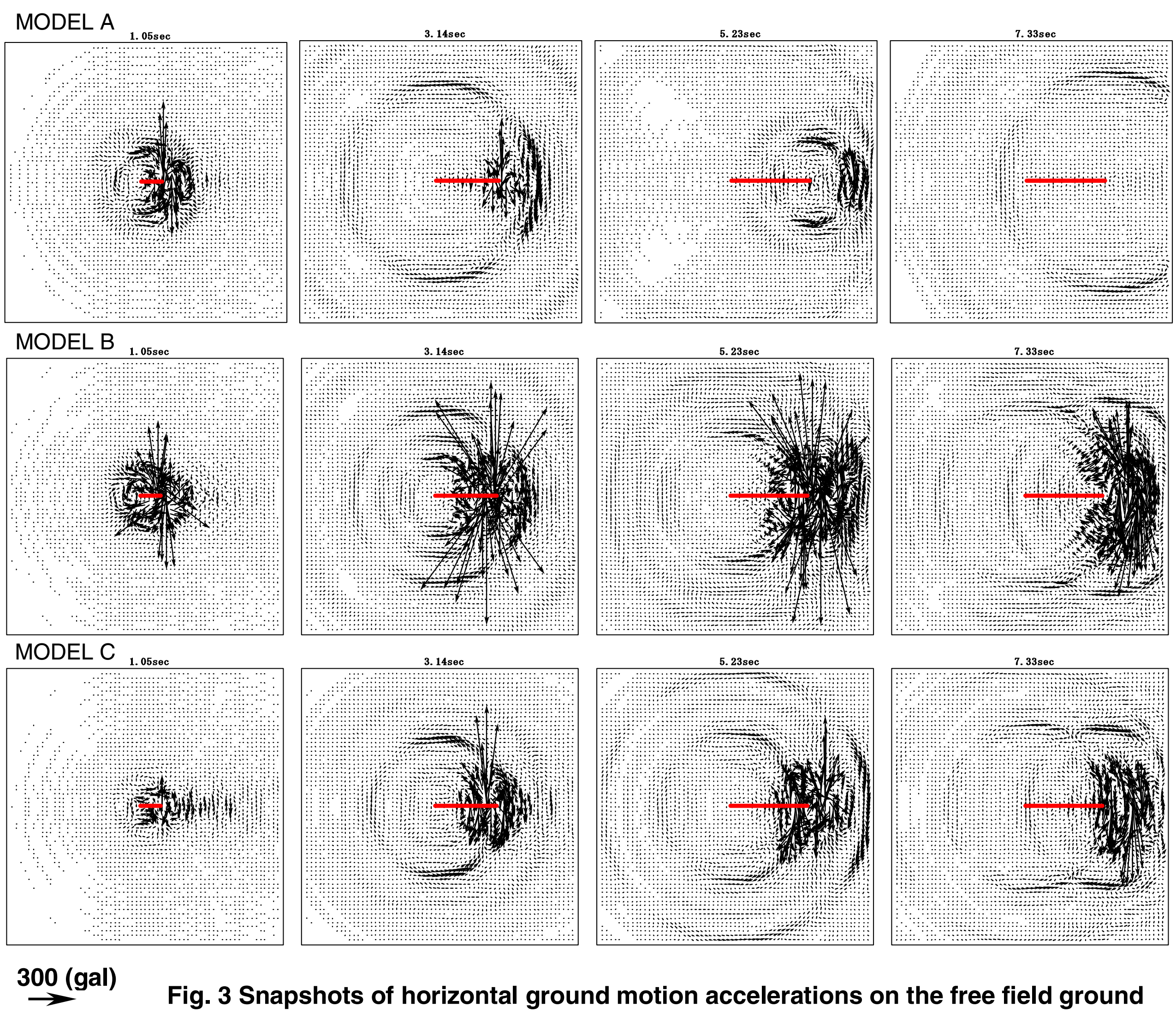

Fig. 3 Snapshots of horizontal ground motion accelerations on the free field ground surface over 30km by 30km area near the strike slip fault, at 4 time instants, for the models A, B and C

The projection line of the vertical strike slip fault to the ground surface is indicated in the central portion of Fig.3 by the black belt. The rupture of the fault starts at $t = 0\sec$ and ends at $t = 3.86\sec(L/Vr)$. The arrow indicates the amplitude and direction of the horizontal ground motion accelerations at each point on the ground surface in the case of average slip dislocation of fault $D = 1.3m$.

It is observed from Fig.3 in common for the 3 models A, B and C that the several vortexes appear around the rupturing fault, and the large accelerations, especially in the fault normal direction (v) present in the tip portion of the fault rupture. The amplitudes and directions of horizontal ground motion accelerations are quite different depending on the 3 models A, B and C, indicating the strong influence of the thickness of the sedimentary layer upon the characteristics of the ground motions. The amplitude of ground accelerations from the model B is the biggest and the smallest from the model A. It is also observed from Fig.3 that the spatial variation of ground motion accelerations near the fault is quite large and complex. The complex nature of the spatial and temporal variation as shown in Fig.3 looks like the vortexes appearing behind an obstacle in the air or water flow. This complex nature of ground motions may be the composite results of the dislocation of the source rupture mechanism (the double coupled forces acting on the dislocation of fault surface) and the seismic wave propagations in the sedimentary layer and the bedrock.

INPUT GROUND MOTIONS TO THE VIADUCT NEAR THE FAULT AND METHOD OF RESPONSE ANALYSIS

Input ground motions to the viaduct

In order to capture the important features of the response behaviors of long continuous viaduct near the strike slip fault rupture, we performed the two cases; the one is a continuous viaduct crossing the strike slip fault, the other case is the continuous viaduct running parallel to the strike slip fault as shown in Figs.4a and 4b. In each case the black circles indicate the number of the piers. The same idealized uniform continuous viaduct models used in the previous study Harada and Nonaka [1], having the total length of 8040m with each span length of 60m, is also adopted in this study. This viaduct is consistent of 134 uniform spans ($8040m/60m$) and 135 uniform piers.

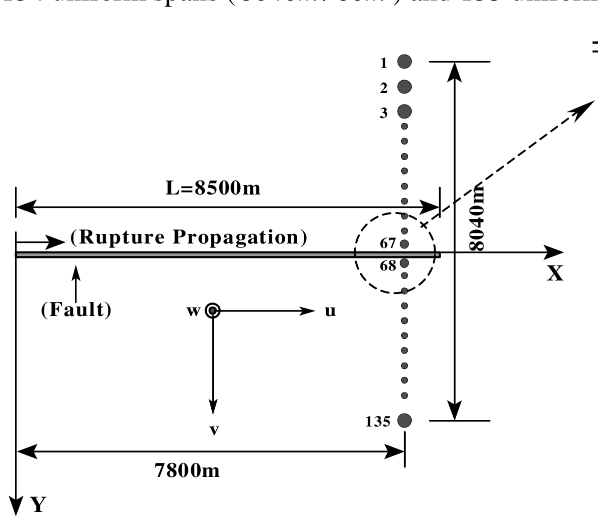

Fig. 4a Plan view of location of the piers of the viaduct crossing the fault

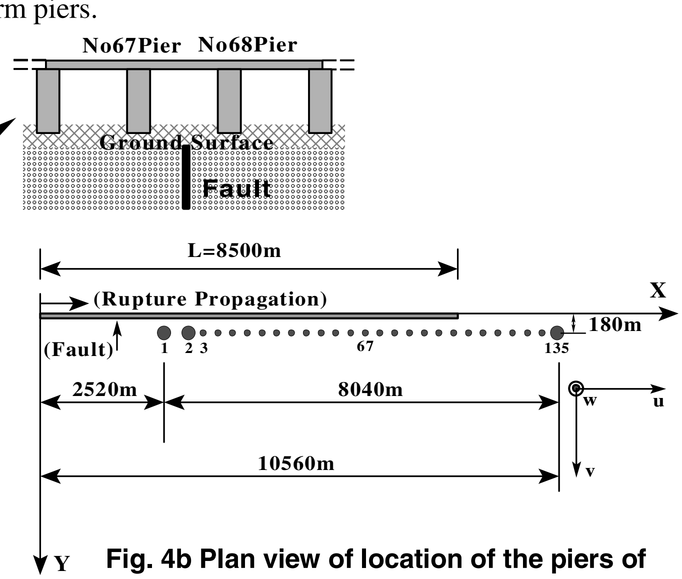

Fig. 4b Plan view of location of the piers of the viaduct running parallel to the fault

In the simulation of seismic ground motions, the 6 components of free field ground motions, consisting of the 3 translational motions (u, v, w) and the 3 rotational motions ($\omega_x, \omega_y, \omega_z$) around the 3 coordinate axes in the Cartesian coordinate system (x, y, z where the x and y plane corresponds to the free field ground surface, and z axis expresses the depth from the free field ground surface), are simulated, Harada et al. [5].

Figure 5 shows the examples of the six components of input ground motions at the 67^{th} pier, which is the closest pier to the fault projection line of the viaduct crossing the fault, as shown in Fig.4a. The 3 translational ground motion accelerations (u, v, w), which correspond to the transverse, longitudinal and vertical directions to the axis of viaduct (see Fig.4a), for the 3 models A, B and C are shown in Fig.5a, while the 3 translational components of ground motion displacements are shown in Fig.5b. Figures 5c and 5d show the 3 rotational components of ground motion accelerations and displacements.

For the case of the model A, the ground motion accelerations are characterized as shows in Fig.5a, by the well defined, discrete single pulse with amplitude of about 1.2G and with frequency of about 1.5Hz appearing in the transverse component u to the bridge axis. This component of ground motion displacement is also characterized as shown in Fig.5b by the large permanent displacement, by reflecting the dislocation pattern of the left lateral slip of the fault.

On the other hand, for the models B and C, the translational ground motion v, which is the longitudinal component of the bridge axis (see Fig.4a), is extremely large in the ground motion acceleration and displacement, but the permanent displacement in this component v is very small compared with that of the translational ground motion u appeared in the model A. The large amplitude of ground acceleration, 1.8G, can be observed in the longitudinal component v in the case of model B as shown in Fig.5a.

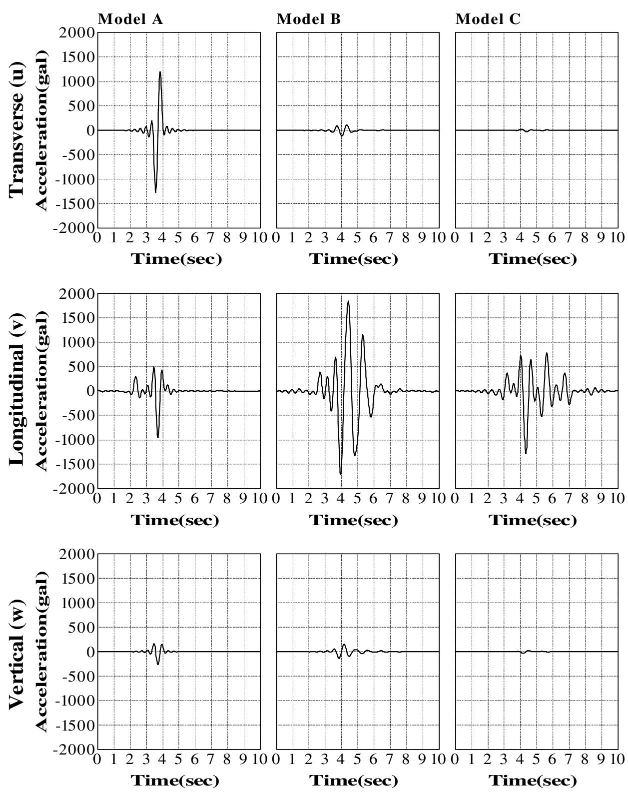

Fig. 5a 3 translational components of input motion accelerations at the 67^{th} pier of the viaduct crossing the fault

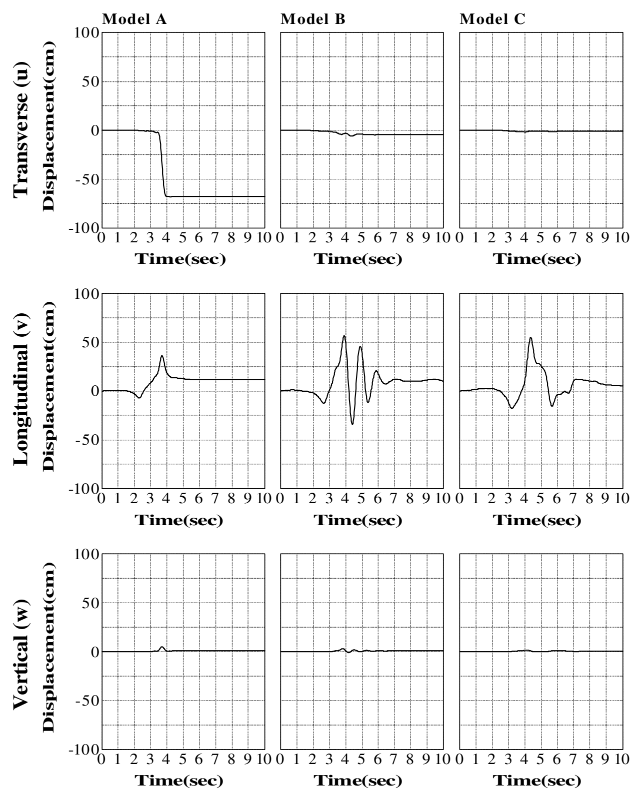

Fig. 5b 3 translational components of input motion displacements at the 67^{th} pier of the viaduct crossing the fault

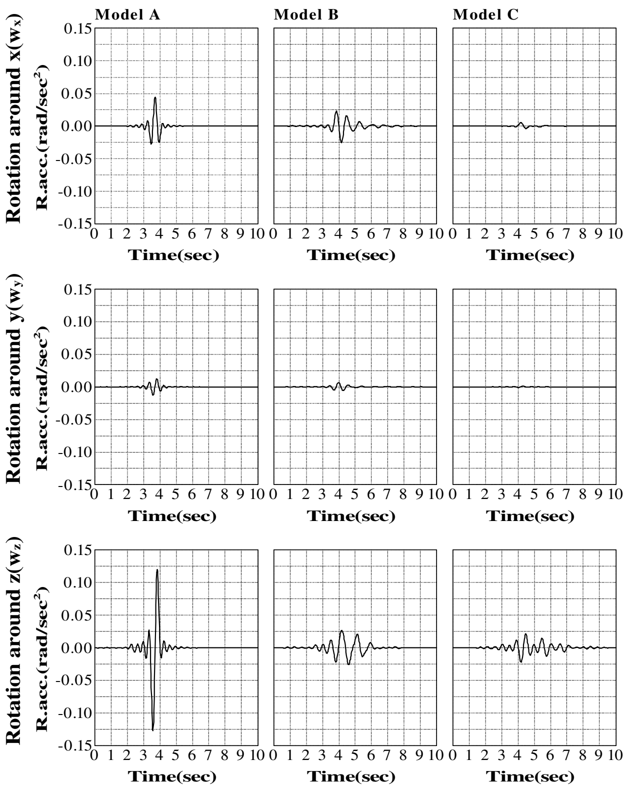

Fig. 5c 3 rotational components of input motion accelerations at the 67th pier of the viaduct crossing the fault

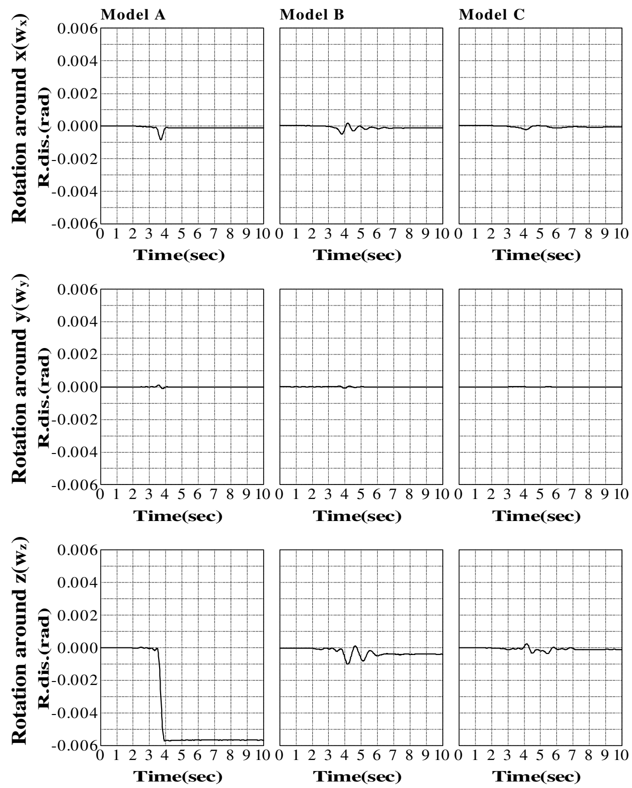

Fig. 5d 3 rotational components of input motion displacements at the 67th pier of the viaduct crossing the fault

Figure 6 shows the response acceleration spectra for the 5% of the critical damping of the total 135 input ground motion accelerations for the case of the viaduct crossing the fault, and Fig.7 shows those for the case of the viaduct running parallel to the fault. In model A shown in the left of Fig.6, the values of the response spectra at the structural natural period of 0.1sec, which approximately correspond to the peak input ground accelerations, vary largely depending on the location of the input motions such as 0.15G to 1.02G for the longitudinal component v to the bridge axis, and 0.13G to 1.28G for the transverse component u. However, the shape of the response spectra of all 135 input motions is almost similar, indicating the frequency distribution of all 135 input motions does not strongly depend on the location of the input motions. The similar characteristics of the response spectra of the input motions obtained from the models B and C can be observed from Fig.6, although the values of the response spectra are different from those of the model A.

To show clearly the large spatial variation of all the 135 input ground motion accelerations, the peak ground motion accelerations at each pier are plotted in Figs.8 and 9. It should be noted here that the spatial variation of peak ground motion accelerations of Fig.8 (for the case of the viaduct crossing the fault) is reflecting the facts that the large relative displacement between the very close two points (the 67th pier and the 68th pier) crossing the fault line occurs, and then the very large ground strains generate for the model A, and also that the ground strains may be small for the models B and C since the maximum relative displacement occurs between the long distant two points.

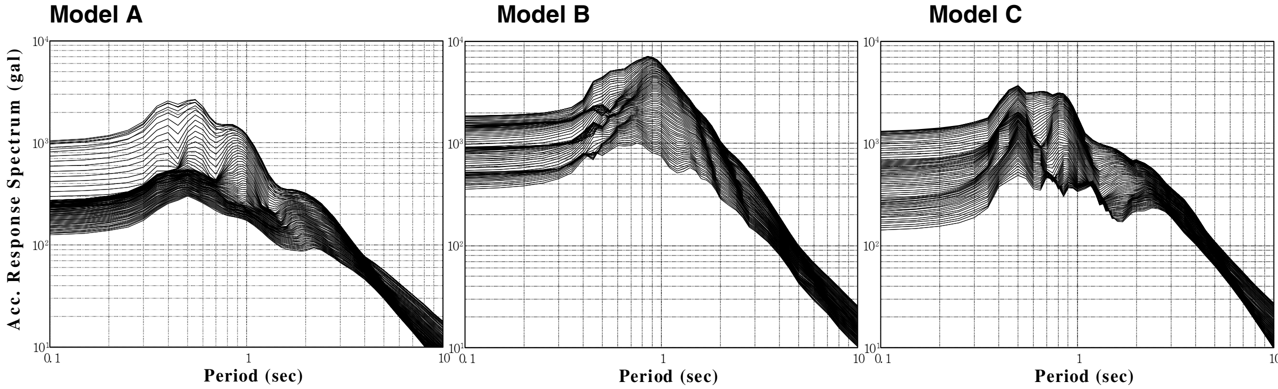

Fig. 6a Response spectra of all 135 input motions for the case of the viaduct crossing the fault (Longitudinal component V, 5% damping)

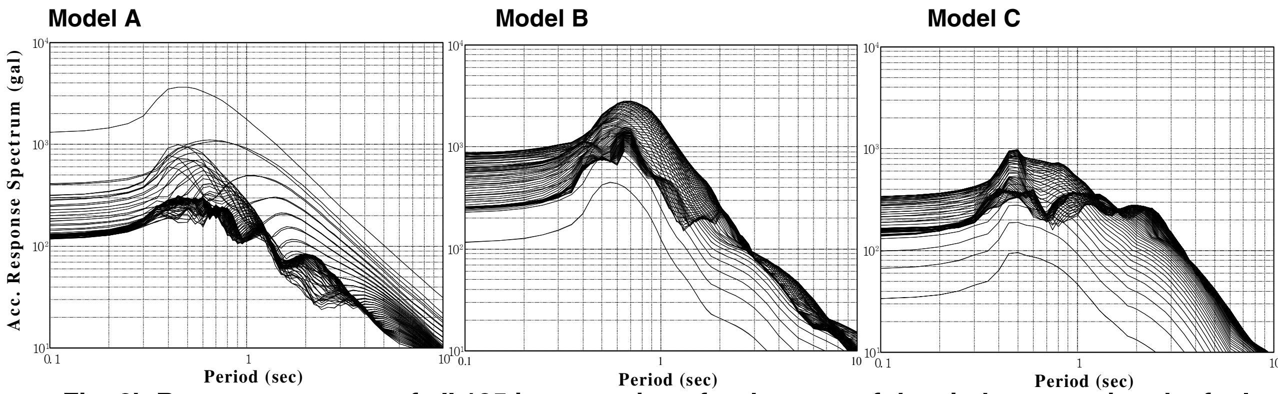

Fig. 6b Response spectra of all 135 input motions for the case of the viaduct crossing the fault (Transverse component U, 5% damping)

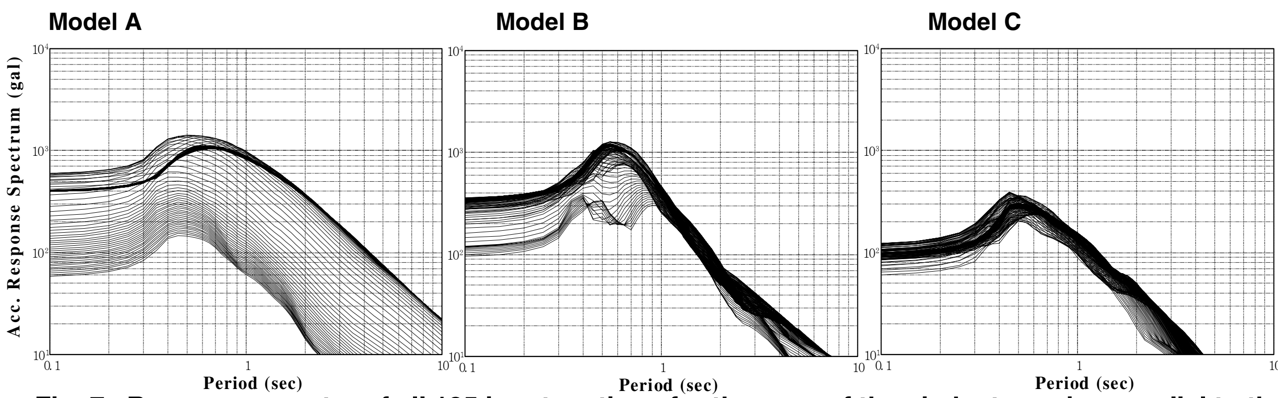

Fig. 7a Response spectra of all 135 input motions for the case of the viaduct running parallel to the fault (Longitudinal component U, 5% damping)

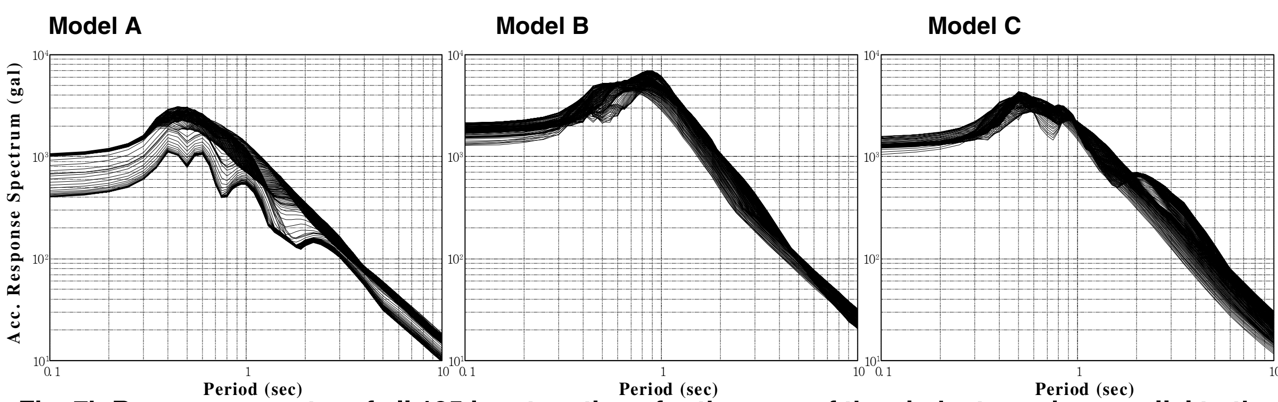

Fig. 7b Response spectra of all 135 input motions for the case of the viaduct running parallel to the fault (Transverse component V, 5% damping)

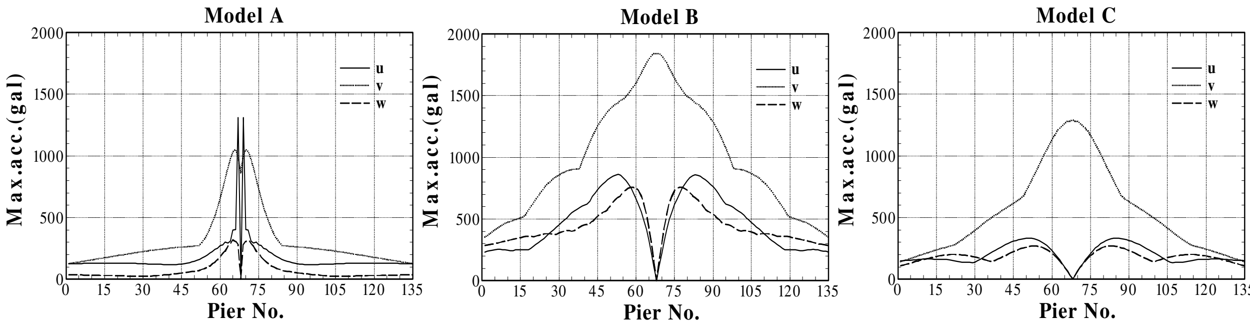

Fig. 8 Spatial distribution of peak accelerations of input motions at all piers of the viaduct crossing the fault

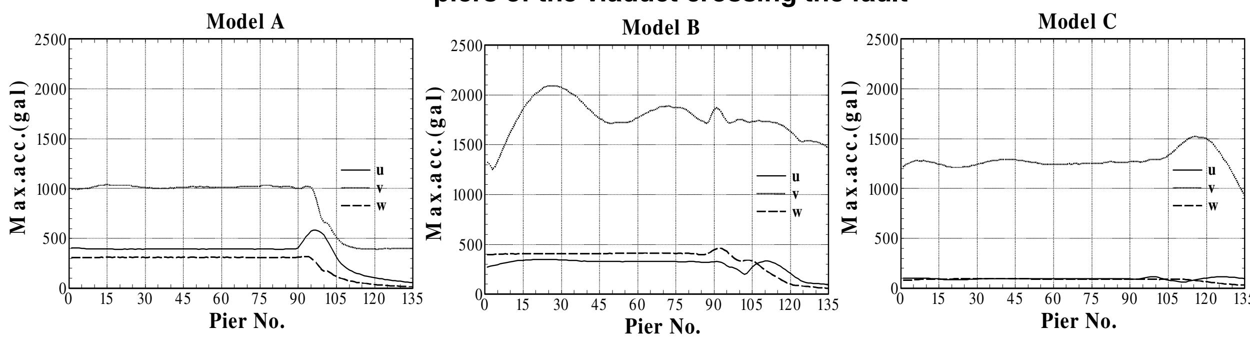

Fig. 9 Spatial distribution of peak accelerations of input motions at all piers of the viaduct running parallel to the fault

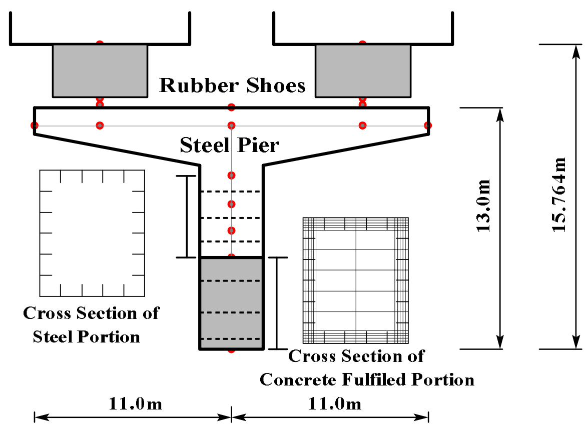

Fig. 10 Cross sectional view of the idealized viaduct

Table 3 Size properties of the idealized viaduct

Number of piers	135
Length of span (m)	60
Height of pier (m)	13.0
Height of C.G of deck (m)	15.764
Height of concrete fulfilled portion (m)	3.65
Total length of viaduct (m)	8040

Idealized continuous viaduct and method of response analysis

Figure 10 and Table 3 show the cross sectional view and the size parameters of the idealized continuous viaduct used in this study. Although the details of this viaduct are described in the previous paper Harada et al. [1][5], the piers are rigidly supported at the bottom by assuming the viaduct is situated on the rock site. The piers are made of steel with rectangle cross section and fulfilled by concrete at the bottom portion of the piers. The piers are discretized by the 3 dimensional fiber elements where the two directional bending moments around longitudinal and transverse axes of the bridge can be incorporated in the inelastic response of the piers. The rotational moment around the vertical axis is modeled by the Saint-Venant assumption. The deck superstructures are modeled by the 3 dimensional elastic frame elements, and these deck superstructures are supported on the rubber shoes modeled by elastic springs. Finally the continuous viaduct is modeled with 3234 three dimensional frame elements and 3101 lumped masses.

Responses of the viaduct were computed by using the computer code Y-FIBET3D [4]. In the computation of responses, the 3 cases are considered; the case 1 corresponds to the 3 dimensional response analysis subjected to the 6 components of ground motions at each bottom of piers, the case 2 is the 3 dimensional response analysis subjected to the 3 translational components of ground motions, and the case 3 is the 2 dimensional response analysis where the transverse or longitudinal component of ground motions at one point, where the maximum acceleration of ground motions is observed, is subjected to all the bottom of piers.

RESULTS OF RESPONSE ANALYSIS OF VIADUCT NEAR THE FAULT

Results of response analysis of the viaduct crossing the fault

In the first, the response behaviors of longitudinal and transverse directions to the bridge axis will be described here. To see the characteristics of response time histories, the response time histories at the several portions of the 67th pier are shown in Fig.11 as an example. It is observed from Fig.11 by comparing with the response time histories at the top of the pier that the response period is elongated by the effect of the rubber shoes such as about 1.1sec period for the transverse response of the model A, and about 1.5sec period for the longitudinal response of model B, in consequence, the long period time histories are observed in the responses of the bending moments at the bottom of the pier. In the case of transverse responses for the model A (surface fault) as shown in Fig.11a, the permanent drifts can be observed in the bottom of the pier due to the permanent dislocation of the fault rupture.

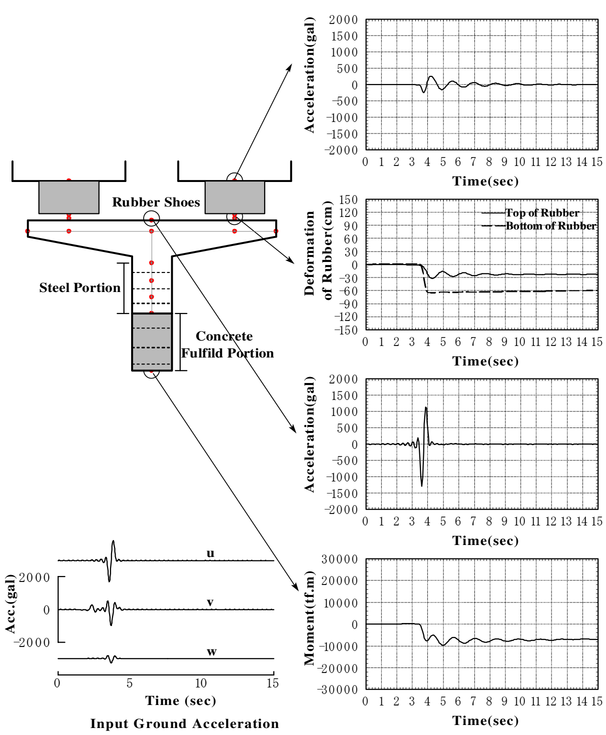

Fig. 11a Response time histories of the 67th pier and the deck for the Model A (Transverse component of the viaduct crossing the fault)

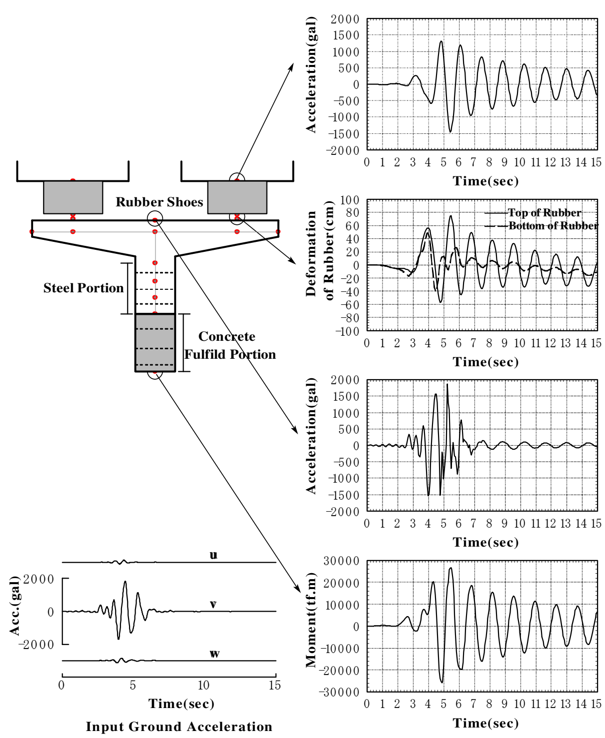

Fig. 11b Response time histories of the 67th pier and the deck for the Model B (Longitudinal component of the viaduct crossing the fault)

To see the overall views of 3D response of total 8040m, the overhead views of the longitudinal response displacements of the continuous viaduct at each 1sec. time instant for the models A, B and C are depicted in Fig.12a. In Fig.12a the response displacements are shown by the vertical lines, because the amplitude and direction of the longitudinal response displacements fall on the bridge axis and cannot be seen if they are depicted in the direction of the bridge axis. Also, the similar overviews of the transverse response displacements for the models A, B and C are shown in Fig.12b.

In the longitudinal response displacements shown in Fig.12a, the deck superstructure moves almost constant along the bridge axis due to its high rigidity in the longitudinal direction of bridge axis, although the displacements of the bottom of each pier vary spatially by reflecting the spatial variation of ground displacements. In the transversal response movements shown in Fig.12b, the deck moves like a shear deformation due to the fault dislocation. For the model A (surface fault), the large shear deformation of the deck occurs in a short distance, because the close two points crossing the surface fault line move in the opposite directions according to the strike slip dislocation, but the shear deformations of the deck obtained from the models B and C show the gentle curves by reflecting the slow spatial variation of the ground motion displacements around the fault projection line to the ground surface.

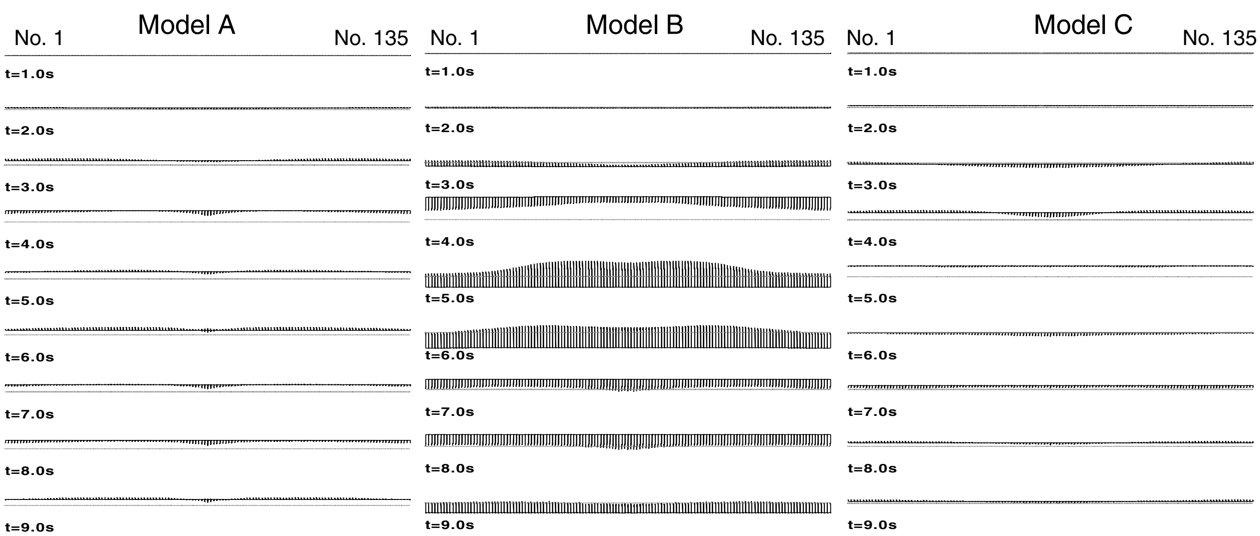

Fig.12a Overhead views of response displacement of the viaduct crossing the fault at each 1sec (Longitudinal component for the Model A, B and C in 3D analysis)

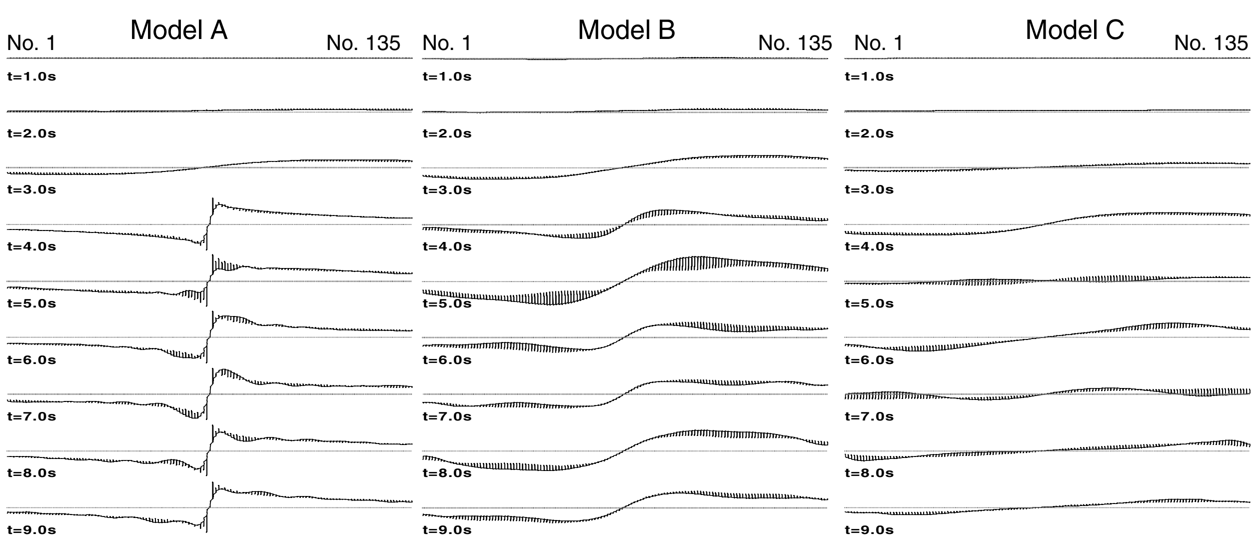

Fig. 12b Overhead views of response displacement of the viaduct crossing the fault at each 1sec (Transverse component for the Model A, B and C in 3D analysis)

This difference of the shear deformations of the deck among the models shown in Fig.12b, is caused by the difference of the distance between two points, where the maximum ground displacement occurs, crossing the fault projection line such as 60m for the model A, about 2km for the model B, and about 3km for the model C.

These results indicate that the existence of the sedimentary layer (Model B and Model C) is the important factor on the response behaviors of the viaduct crossing the fault line, especially on the transversal response behaviors.

As the examples of the overhead views of the deformations of the viaduct obtained from the 2D analysis where the ground motion at one location, in which the maximum ground acceleration occurs, is inputted at all the bottom of the piers, the longitudinal response displacements obtained from the model B, at the time instant 4.80sec in which the maximum response displacement appears, is shown in Fig.13a. The similar overview of the transversal response displacements obtained from the model B, at time 6.30sec is shown in Fig.13b. In the 2D analysis, obviously, the response displacements are constant along the continuous viaduct without reflecting the spatial variation of ground motions.

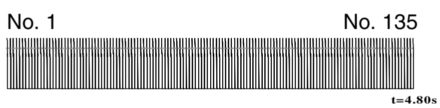

Fig. 13a Overhead views of response displacement of the viaduct at t = 4.80sec (Longitudinal component for the Model B in 2D analysis)

Fig. 13b Overhead views of response displacement of the viaduct at t = 6.30sec (Transverse component for the Model B in 2D analysis)

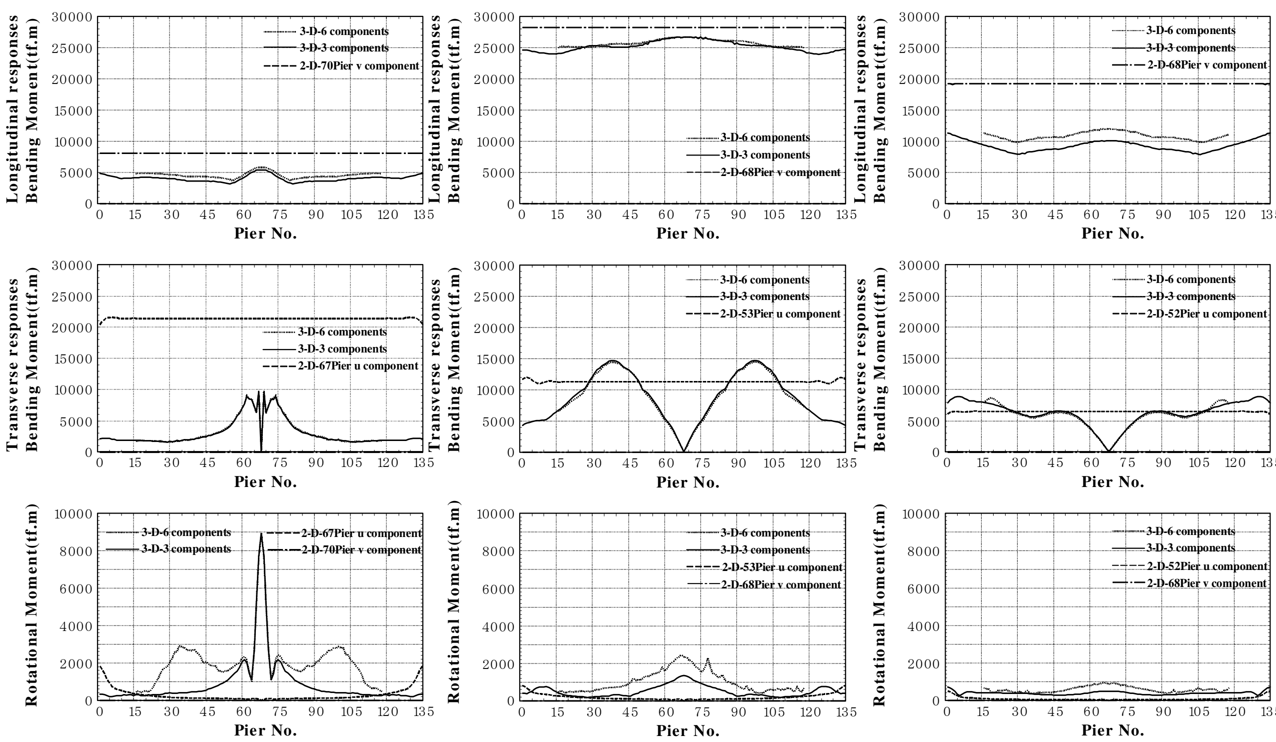

Model A Model B Model C

Fig. 14 Comparison of maximum bending and rotational moments at the bottom of total 135 piers from the 3D analyses (6 components and 3 components of input motions) and the 2D analysis

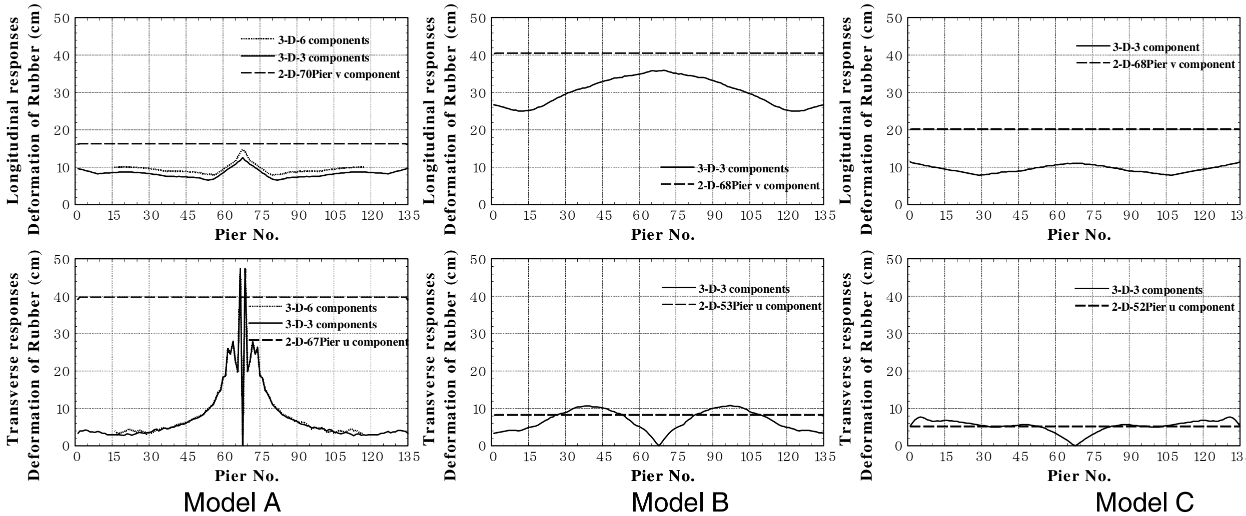

Fig. 15 Comparison of maximum relative deformations of rubber shoes of total 135 piers from the 3D analyses (6 components and 3 components of input motions) and the 2D analysis

As the summary of the response behaviors of the viaduct crossing the fault, the maximum bending moments and the maximum torsional moment of the bottom of piers, and the maximum relative displacements of the rubber shoes at each pier are plotted in Figs.14 and 15. They are obtained from the 3D analysis using the 6 components of input motions, the 3D analysis using 3 translational components input motions, and the 2D analysis for the models A, B and C.

In the first, by comparing the response results shown in Figs.14 and 15 which are obtained from the 3D analyses (the two cases; the 6 components of input motions, and the 3 translational components of input motions) and the 2D analysis, it is found that the responses from the 2D analysis are, on the whole, larger than those from the 3D analyses, except the torsional moments indicated in the bottom line of Fig.14. The quite large torsional moments such as about 9,000tf.m for the model A (surface ground) are generated at the bottoms of the 67th and 68th piers, which locate at the two positions closest to the fault projection line.

In the next, by comparing the response results obtained from the two cases; the 6 components of input motions ($u,v,w,\omega_x,\omega_y,\omega_z$), and the 3 components of input motions (u,v,w), it is found that the differences of the responses are not so large except the torsional response moments. This observation means that the rotational ground motions ($\omega_x,\omega_y,\omega_z$) do not affect on the response except the torsional response moments.

As the summaries of the response behaviors indicated in Figs.14 and 15, it is concluded that the 3D analysis is necessary to capture the response behaviors of the viaduct crossing the fault, and the thickness of the sedimentary layer overlying the upper edge of the fault is the important factor affecting on the response behaviors. Especially, for the model A where the upper edge of the fault reaches to the ground surface, the extremely large torsional moments enough to destroy the piers are generated at the bottom of the piers closest to the fault line.

Results of response analysis of the viaduct running parallel to the fault

This part will describe the response behaviors of the viaduct running parallel to the fault. The overhead views of the longitudinal and transverse response displacements of the continuous viaduct at each 1sec. time instant for the models A, B and C are shown in Fig.16. In the longitudinal response displacements shown in Fig.16a, the deck superstructure moves almost constant along the bridge axis due to its high rigidity in the longitudinal direction of bridge axis, although the displacements of the bottom of each pier vary spatially by reflecting the spatial variation of ground displacements. In the transversal response movements shown in Fig.16b, the deck moves like the movements of a snake. For the model B (0.5km sedimentary layer), the large shear deformation of the deck is observed, as shown in the center column of Fig.16b.

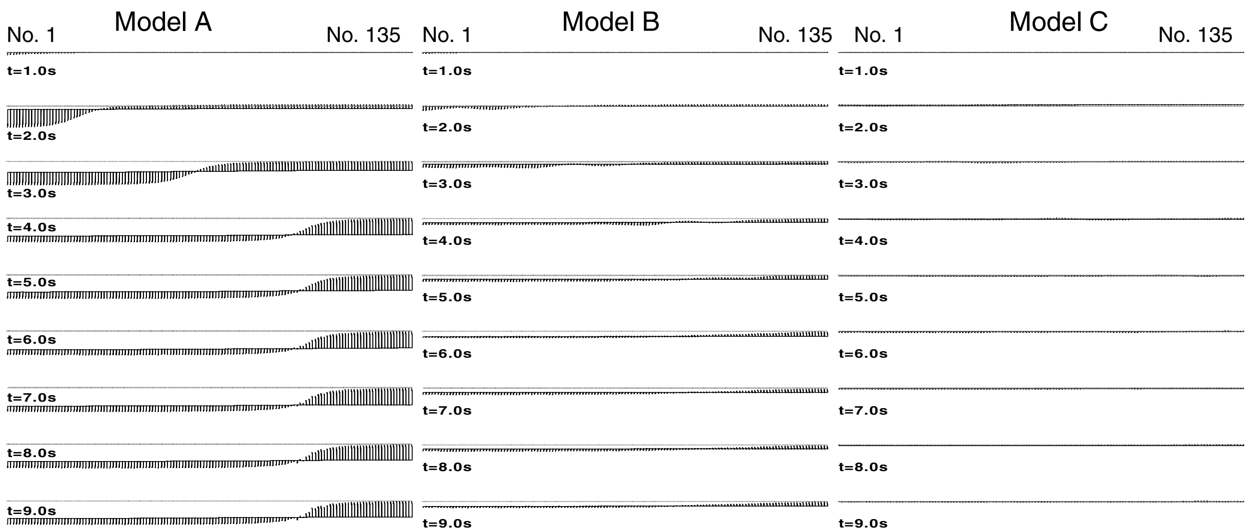

Fig.16a Overhead views of response displacement of the viaduct running parallel to the fault at each 1sec (Longitudinal component for the Model A, B and C in 3D analysis)

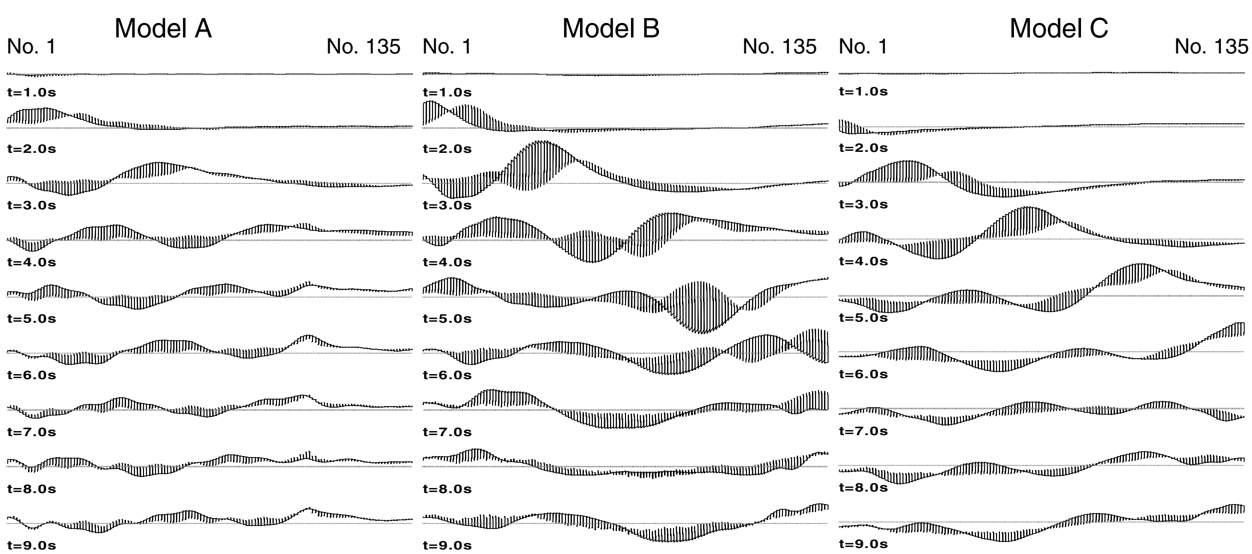

Fig. 16b Overhead views of response displacement of the viaduct running parallel to the fault at each 1sec (Transverse component for the Model A, B and C in 3D analysis)

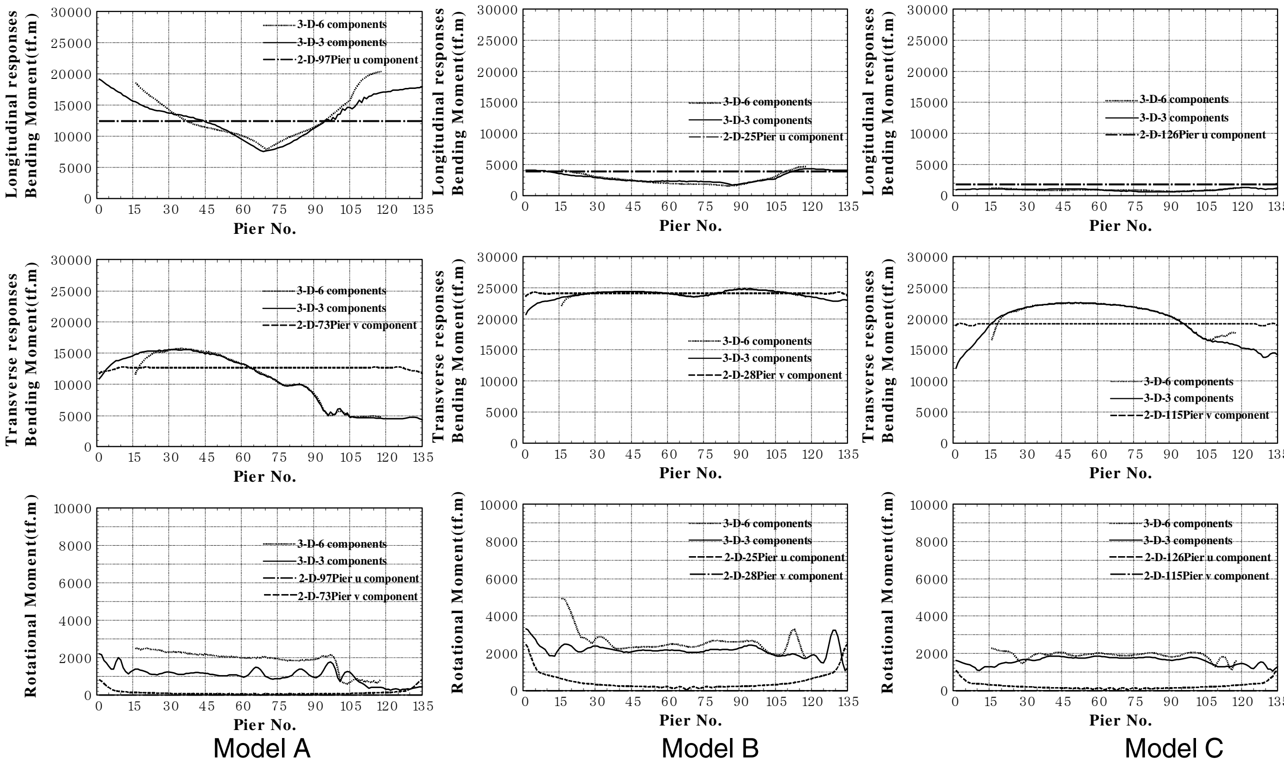

Fig. 17 Comparison of maximum bending and rotational moments at the bottom of total 135 piers from the 3D analyses (6 components and 3 components of input motions) and the 2D analysis

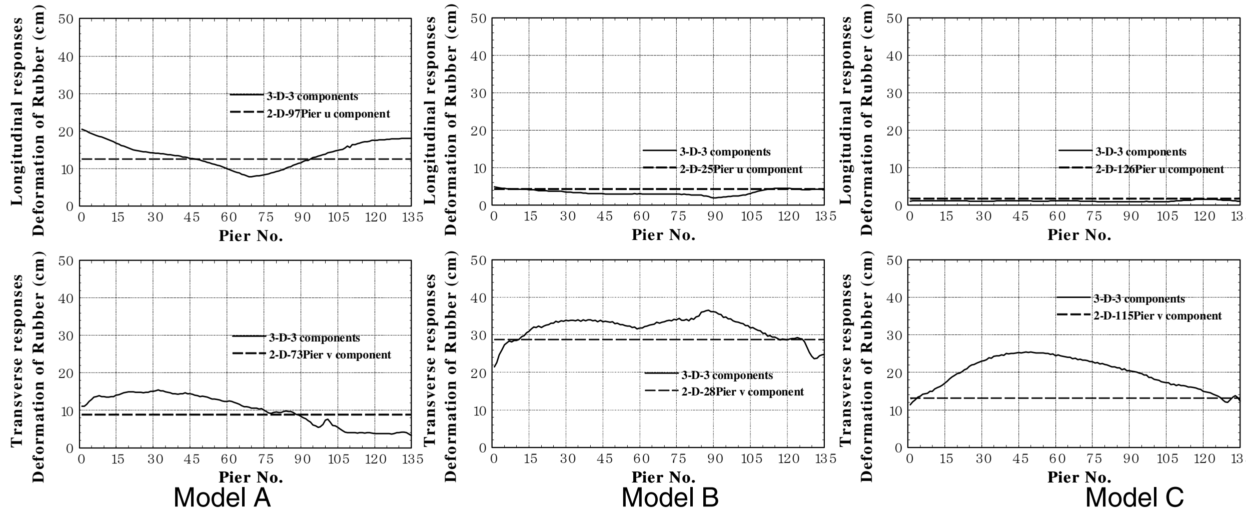

Fig. 18 Comparison of maximum relative deformations of rubber shoes of total 135 piers from the 3D analyses (6 components and 3 components of input motions) and the 2D analysis

In the same way of the previous section, the maximum bending moments and the maximum torsional moment of the bottom of piers, and the maximum relative displacements of the rubber shoes at each pier are plotted in Figs.17 and 18. By comparing the response results shown in Figs.17 and 18, it is found that the response results from the 2D analysis are smaller than those from the 3D analyses, except the bending moment of transverse directional to the bridge axis in model B. Also, it is found that the differences of the responses between the 6 components and the 3 components of input motions are not so large except the torsional response moments. This observation means that the rotational ground motions ($\omega_x, \omega_y, \omega_z$) do not affect on the responses except the torsional response moments.

From the response behaviors indicated in Figs.17 and 18, it is concluded that the 3D analysis is necessary to capture the response behaviors of the viaduct running parallel to the fault, and the thickness of the sedimentary layer overlying the upper edge of the fault is the important factor affecting on the response behaviors. Especially, for the models B and C where the large bending moments in the transverse direction to bridge axis such as about the 25,000tf.m and 23,000tf.m are generated at the bottom of piers.

CONCLUSIONS

Numerical examples of the near fault ground motions for a strike slip fault, by changing the thickness of the sedimentary layer overlying the fault, were presented. They were obtained from a computer simulation using a stiffness matrices based formulation of the physical processes of propagation of the seismic waves generated by a kinematic model of fault rupture in laterally homogeneous layered media. It is found that the several vortexes, like those appearing behind an obstacle in an air or water flow, appear in the seismic wave field on the free field ground surface, in consequence the spatial and temporal variation of ground motions are large and complex, strongly depending on the thickness of the sedimentary layer.

In order to capture the important features of response behaviors of an idealized continuous viaduct near the strike slip fault rupture, we examined the two cases; the one is a continuous viaduct crossing the fault, the other case is the continuous viaduct running parallel to the fault, and performed the inelastic response analyses using the 3 dimensional fiber element models. It is found that the thickness of the sedimentary layer strongly affects on the response behaviors of the viaduct near the fault. In surface fault case, model A, where the upper edge of the fault rupture reaches to the ground surface, the large torsional moments are generated at the bottom of piers of the viaduct crossing the fault.

In other words, the existence of the sedimentary layer overlying the fault drastically reduces the torsional moments of the bottom of piers in the case of the viaduct crossing the fault. In case of the viaduct running parallel to the fault, the large bending moments of the piers are generated in the transverse direction to the bridge axis for the models B and C, where the sedimentary layers exist with thickness of 0.5km and 1.5km. Of course, the 3D analysis is necessary to capture the response behaviors of a viaduct near a fault.

REFERENCES

1. Harada T. and Nonaka T. “Seismic response characteristics of a continuous viaduct near a strike slip fault.” Journal of Structural Engineering, JSCE, Japan, 47A: 843-849, 2001, in Japanese.
2. Harada T., Ohsumi T. and Okukura H. “Analytical solutions of wave field in 3-dimensional Cartesian coordinate and their application to synthesis of seismic ground motions.” Journal of Structural Mechanics and Earthquake Engineering, JSCE, Japan, No.612/I-46: 99-108, 1996, in Japanese.
3. Harada T. and Yamashita H. “Stiffness matrices based simulation of ground motion and vortex of seismic wave field near a fault.” Journal of Applied Mechanics, JSCE, Japan, Vol.3: 569-576, 2000, in Japanese.
4. Computer Code Y-FIBER3D, Yamatosekei Company Ltd. , Japan, 1995.
5. Harada T., Oho K., Nonaka T. and Ohsumi T., “3-dimensional response behaviors of a viaduct near a fault.” Proc. of the 11th Japan Earthquake Engineering Symposium, CD-ROM Paper no. 296. , 2002, in Japanese.